AGU PUBLICATIONS

JGR

Journal of Geophysical Research: Atmospheres

RESEARCH ARTICLE
10.1002/2016JD024860

Key Points:
- Two approaches to model subgrid diffusion at grey zone resolutions are compared in simulating two cases of an evolving boundary layer
- Bounding approach significantly improves spin-up; blending better simulates early morning profiles
- Proposed methods exhibit particular strengths and weaknesses indicating the level of compromise currently needed in high-resolution NWP

Correspondence to:
G. A. Efstathiou,
G.Efstathiou@exeter.ac.uk

Citation:
Efstathiou, G. A., R. J. Beare, S. Osborne, and A. P. Lock (2016), Grey zone simulations of the morning convective boundary layer development, *J. Geophys. Res. Atmos.*, *121*, doi:10.1002/2016JD024860.

Received 26 JAN 2016
Accepted 16 APR 2016
Accepted article online 23 APR 2016

Grey zone simulations of the morning convective boundary layer development

G. A. Efstathiou[1], R. J. Beare[1], S. Osborne[2], and A. P. Lock[3]

[1]Department of Mathematics, Centre for Geophysical and Astrophysical Fluid Dynamics, University of Exeter, Exeter, UK, [2]Met Office Field Site, Cardington Airfield, Bedford, UK, [3]Met Office, Exeter, UK

Abstract Numerical simulations of two cases of morning boundary layer development are conducted to investigate the impact of grid resolution on mean profiles and turbulent kinetic energy (TKE) partitioning from the large eddy simulation (LES) to the mesoscale limit. Idealized LES, using the 3-D Smagorinsky scheme, is shown to be capable of reproducing the boundary layer evolution when compared against measurements. However, increasing grid spacing results in the damping of resolved TKE and the production of superadiabatic temperature profiles in the boundary layer. Turbulence initiation is significantly delayed, exhibiting an abrupt onset at intermediate resolutions. Two approaches, the bounding of vertical diffusion coefficient and the blending of the 3-D Smagorinsky with a nonlocal 1D scheme, are used to model subgrid diffusion at grey zone resolutions. Simulations are compared against the coarse-grained fields from the validated LES results for each case. Both methods exhibit particular strengths and weaknesses, indicating the compromise that needs to be made currently in high-resolution numerical weather prediction. The blending scheme is able to reproduce the adiabatic profiles although turbulence is underestimated in favor of the parametrized heat flux, and the spin-up of TKE remains delayed. In contrast, the bounding approach gives an evolution of TKE that follows the coarse-grained LES very well, relying on the resolved motions for the nonlocal heat flux. However, bounding gives unrealistic static instability in the early morning temperature profiles (similar to the 3-D Smagorinsky scheme) because model dynamics are unable to resolve TKE when the boundary layer is too shallow compared to the grid spacing.

1. Introduction

The first computerized weather forecast was produced in the early 1950s using a rather coarse horizontal domain of 15 × 18 grid points over North America (with a grid spacing of about 736 km at 45°N) [*Charney et al.*, 1950]. Since then grid resolution in numerical weather prediction (NWP) models has been increasing in connection with available computing resources and is now moving toward the very fine *O*(1 km) horizontal resolution. Numerical models can now be run with extensively dense computational grids on massively parallel computing systems, enabling dynamics to resolve subsynoptic scales and most of the mesoscale variability. With increasing grid resolution, simulations (with grid lengths comparable to the depth of the troposphere) first start to resolve deep convective clouds where explicit microphysics remove some of the convective instability from the troposphere in expense of the convective parametrization. At resolutions in the range of 1 to 10 km lies the grey zone for the moist convective processes [*Arakawa and Wu*, 2013] where clouds are only partially explicitly simulated as the intercloud separation scale is not adequately resolved.

However, as regional models are now approaching the subkilometric scale, boundary layer (BL) turbulence becomes also partially resolved, imposing significant challenges in the formulation of subgrid turbulence parametrizations. In the BL grey zone, the energy-containing turbulence scales are comparable to the grid scale [*Wyngaard*, 2004; *Beare*, 2014] and as a result neither large eddy simulation (LES) nor mesoscale parametrizations are suitable for the BL modeling over this range of grid resolutions. Traditional 1D BL nonlocal parametrizations [e.g., *Lock et al.*, 2000; *Hong et al.*, 2006] seem to remove too much energy from the resolved to the unresolved scales [*Honnert et al.*, 2011; *Shin and Hong*, 2013, 2015]. Moreover, the partitioning of turbulent kinetic energy (TKE) when using the 3-D Smagorinsky closure depends on the choice of the turbulence mixing length [*Efstathiou and Beare*, 2015]. Increasing mixing length leads to the damping of any resolved motions, while reducing its magnitude results in enhanced convective overturning usually on the grid scale [*Beare*, 2014; *Efstathiou and Beare*, 2015]. In any case the Smagorinsky scheme is only a rough

approximation of the complete turbulent transport equations [*Wyngaard*, 2004] intended to model isotropic subgrid motions although using the appropriate mesoscale mixing length can be considered akin to a 1D local BL scheme.

In order to derive a reference transition pattern of the turbulent kinetic energy (TKE) from the LES to the mesoscale limit, *Honnert et al.* [2011] coarse grained a series of different LES case studies to obtain the intermediate resolution filtered fields. A new similarity relationship was introduced that described the partitioning of the turbulent fluxes to resolved and subgrid components. Using this approach, *Boutle et al.* [2014] blended the 3-D Smagorinsky with a 1D nonlocal BL scheme to simulate a stratocumulus case at grey zone resolutions. The blending scheme is now used operationally within the Met Office Unified Model (MetUM) to provide seamless predictions across the scales. In a similar way *Shin and Hong* [2015] modified the conventional nonlocal *K*-profile scheme [*Hong et al.*, 2006] to account for the grid-size dependency of local and nonlocal fluxes after diagnosing their relative contribution across the grey zone according to *Shin and Hong* [2013]. *Ito et al.* [2015] extended the Mellor-Yamada level-3 scheme to grey zone resolutions by modifying the various length scales using statistics obtained from the coarse-grained LES fields.

Efstathiou and Beare [2015] attempted to quantify subgrid diffusion in the grey zone, comparing coarse-grained LES of a convective BL (CBL) with actual independent simulations for different grid resolutions. A new approach was developed based on bounding of the vertical diffusion to its effective values while adopting a mesoscale 2-D treatment for horizontal diffusion. It was shown that the bounding was able to follow the theoretical TKE transition pattern across the scales, reproducing the main characteristics of the coarse-grained fields. Additionally, this comparison demonstrated the physical constraints of permitting some convective overturning beyond the LES limit. Reducing mixing length values in the 3-D Smagorinsky scheme led to significantly stronger turbulent fluctuations with smaller-scale structures compared to the coarse-grained fields. In contrast, the bounding approach matched the energetics of the filtered fields as enhanced horizontal diffusion removed the grid-scale dependency. *Ching et al.* [2014] also showed that overenergetic secondary mesoscale circulations were developed when a numerical model was used at grey zone resolutions after spin-up time was reached [see also *Zhou et al.*, 2014].

As many of these studies have been conducted under steady state conditions [*Shin and Hong*, 2013, 2015; *Beare*, 2014; *Efstathiou and Beare*, 2015; *Ito et al.*, 2015] where turbulence is already developed, it is crucial to examine the behavior of the proposed parametrizations under time-dependent heat fluxes and a deepening BL such as the case of the morning CBL growth over land. *Zhou et al.* [2014] examined the development of a CBL at grey zone resolutions using the Wangara day 33 case study and identified the Rayleigh number as the controlling parameter in determining the onset of turbulence at different horizontal resolutions. The dependence of turbulence initiation on grid spacing can have significant implications in the simulation of shallow convection especially the onset and strength of thermal convection which in turn can influence the transition from shallow to deep convection.

In this work, two case studies of the morning CBL development are simulated with the Met Office Large Eddy Model (LEM), from the LES to the mesoscale limit using the standard 3-D Smagorinsky turbulence scheme. The first case study adopted is the well-studied Wangara day 33 case, of a deep BL over south-east Australia and a spring, shallow BL development over the Cardington Met Office site in Bedford, UK (52.105°N, 0.422°W). First- and second-order quantities are examined and compared with the available measurements, while two pragmatic approaches, the bounding of the vertical diffusion coefficient and the blending of the 3-D Smagorinsky with a 1D nonlocal *K* profile scheme, are implemented in the LEM at grey zone resolutions. The behavior of the parametrizations is examined during the morning growth of the BL, testing their ability in reproducing basic meteorological LES profiles as well as the resolved TKE evolution compared to the coarse-grained LES fields. The onset of resolved turbulent fluctuations at grey zone resolutions is shown to be very sensitive to the choice of the subgrid scheme. Differences in turbulence spin-up reveal significant interactions between the treatment of subgrid diffusion and model dynamics at grey zone resolutions.

2. The LEM Formulation

The LEM version 2.4 was used for the simulations conducted in this study. Here the Navier-Stokes equations with the Boussinesq approximation are solved in 3-D using a centered-difference advection scheme

[*Piacsek and Williams*, 1970] for the momentum and the total variation diminishing scheme [*Leonard et al.*, 1993] for the heat equation. The momentum equation in tensor notation has the following form [see *Brown*, 1999]

$$\frac{\partial \overline{u}_i}{\partial t} + \overline{u}_j \frac{\partial \overline{u}_i}{\partial x_j} = -\frac{1}{\rho_s}\frac{\partial \overline{P}}{\partial x_i} - \frac{1}{\rho_s}\frac{\partial P_0}{\partial x_i} + f\left(\delta_{i1}\overline{u}_2 - \delta_{i2}\overline{u}_1\right) + \delta_{i3} g \frac{\overline{\theta}''}{\theta_0} - \frac{\partial \overline{u_i' u_j'}}{\partial x_j}, \tag{1}$$

where $\overline{u}$ is the filtered (resolved) velocity vector, $\overline{P}$ is the pressure, ρ_s is air density, $\partial P_0/\partial x_i$ is a large-scale pressure gradient corresponding to an imposed geostrophic wind, f is the Coriolis parameter, δ is the Kronecker delta, $\overline{\theta}''$ is the perturbation of the resolved potential temperature ($\overline{\theta}$) from its horizontally averaged value, θ_0 is the reference potential temperature, g is the gravitational acceleration, and $\overline{u_i' u_j'}$ is the subgrid (subfilter) momentum flux. The heat equation is given by

$$\frac{\partial \overline{\theta}}{\partial t} + \overline{u}_j \frac{\partial \overline{\theta}}{\partial x_j} = -\frac{\partial \overline{u_j' \theta'}}{\partial x_j}. \tag{2}$$

The only source of heat in the simulations is the subgrid sensible heat flux ($\overline{u_j' \theta'}$). Flow is considered incompressible according to the relationship

$$\frac{\partial \overline{u}_j}{\partial x_j} = 0. \tag{3}$$

2.1. The 3-D Smagorinsky Scheme

The contribution of the subgrid fluxes on the momentum and heat equations in the LEM is modeled using the 3-D Smagorinsky scheme [*Brown et al.*, 1994]. This scheme is proportional to a first-order closure of the full transport equations [*Wyngaard*, 2004] and is suitable for modeling the inertial subrange at LES resolutions. However, it has been used at grey zone resolutions especially in deep convection studies [e.g *Pearson et al.*, 2014]. The subgrid momentum flux is given by

$$\overline{u_i' u_j'} = -K_M S_{ij}, \tag{4}$$

the subgrid turbulent heat flux is specified by

$$\overline{u_j' \theta'} = -K_H \frac{\partial \overline{\theta}}{\partial x_j}, \tag{5}$$

where K_M and K_H is the momentum and heat diffusivity, respectively. The rate of the strain tensor S_{ij} is given by

$$S_{ij} = \frac{\partial \overline{u}_i}{\partial x_j} + \frac{\partial \overline{u}_j}{\partial x_i}. \tag{6}$$

Eddy diffusivities (K_M, K_H) are equal to

$$K_M = l^2 S f_M(Ri) \tag{7}$$

$$K_H = l^2 S f_H(Ri), \tag{8}$$

where S is the modulus of S_{ij} , f_H and f_M are the stability functions for momentum and heat, respectively, as functions of the Richardson number (Ri) [see *Brown et al.*, 1994]. The neutral mixing length (l) is calculated as

$$\frac{1}{l^2} = \frac{1}{(kz)^2} + \frac{1}{\lambda^2} \tag{9}$$

here z is the distance from the ground, k is the von Karman constant, and λ is the basic mixing length specified as

$$\lambda = c_S \Delta x, \tag{10}$$

where c_S is the Smagorinsky constant equal to 0.23 in this study and Δx is the horizontal grid spacing.

2.2. The Bounding Approach

The bounding approach [*Efstathiou and Beare*, 2015] is based on conserving the inherent diffusivity of the flow across the scales. In this manner, the diffusion coefficient is restricted on the vertical to the effective diffusivity

values of the flow field at the LES limit that is well approximated by the vertical K profile [*Troen and Mahrt*, 1986; *Hong et al.*, 2006].

$$K_{M(1D)} = \begin{cases} kw_s z\left(1-\frac{z}{z_h}\right)^2, & \text{if } z < z_h. \\ 0, & \text{otherwise} \end{cases} \tag{11}$$

and

$$K_{H(1D)} = \frac{K_{M(1D)}}{\mathrm{Pr}}, \tag{12}$$

where w_s is a mixed-layer velocity scale [*Noh et al.*, 2003] and Pr is the Prandtl number (Pr = 0.6). The BL depth (z_h) is considered to be at the height of the local minimum of the vertical resolved heat flux. If no turbulent fluctuations are resolved, the BL depth is set at the first level where $Ri > 0.5$. The diffusion coefficients for momentum and heat are then calculated as the minimum between the 1D K profile and the 3-D Smagorinsky scheme (equations (7) and (8))

$$K_M = \min[K_{M(1D)}, K_M(Ri)] \tag{13}$$

$$K_H = \min[K_{H(1D)}, K_H(Ri)]. \tag{14}$$

Horizontal diffusion is handled by equations (7) and (8) using a 2-D form of the local wind shear (S). Momentum and heat fluxes are calculated according to equations (4) and (5).

2.3. Blending of the 3-D Smagorinsky With a *K*-Profile Nonlocal BL Scheme

Following the derivation of the partial similarity functions proposed by *Honnert et al.* [2011] that describe the transition of the subgrid fluxes at grey zone resolutions, *Boutle et al.* [2014] blended the 3-D Smagorinsky with a nonlocal K-profile scheme to model subgrid fluxes from the LES to the mesoscale limit. The blending function they used (W_{1D}) has the following form:

$$W_{1D} = 1 - \tanh\left(\beta\frac{z_{\mathrm{turb}}}{\Delta x}\right)\max\left[0, 1-\frac{\Delta x}{4z_{\mathrm{turb}}}\right], \tag{15}$$

where $z_{\mathrm{turb}} = z_h$ in the cloud-free BL and $\beta = 0.15$ [*Boutle et al.*, 2014]. Sensitivity tests using a range of β values that correspond to the 5th/95th percentile of the distribution of *Honnert et al.* [2011] LES data revealed that the impact of β on model results was limited. First, equation (15) is used to blend between the Smagorisnky (l) and a mesoscale (l_{1D}) mixing length

$$l_{\mathrm{blend}} = W_{1D}l_{1D} + (1 - W_{1D})l \tag{16}$$

with

$$\frac{1}{l} = \frac{1}{kz} + \frac{1}{\lambda_0} \tag{17}$$

where $\lambda_0 = \max[40, 0.15z_h]$. The diffusion coefficients are then calculated [*Lock et al.*, 2000; *Boutle et al.*, 2014]

$$K_M = \max\left[W_{1D}K_{M(1D)}, l^2_{\mathrm{blend}}Sf_M(Ri)\right] \tag{18}$$

$$K_H = \max\left[W_{1D}K_{H(1D)}, l^2_{\mathrm{blend}}Sf_H(Ri)\right]. \tag{19}$$

A simpler approach is used in the implementation of the blending scheme in the LEM compared to *Boutle et al.* [2014], adopting the same K-profile relationships as the bounding scheme to make the intercomparison between the different parametrizations more straightforward. Calculation of z_h follows the iterative procedure of *Holtslag and Boville* [1993], *Hong and Pan* [1996], and *Hong et al.* [2006] comparing at each model level the bulk Ri with the critical bulk Ri (=0.0 here). Subgrid momentum fluxes are calculated according to equation (4) and considered local in this study. However, for the subgrid heat flux parametrization a nonlocal part is added

expressed by a countergradient term (γ) and an explicit representation of entrainment ($\overline{w'\theta}_{z_h}$) that has the following form [see also *Boutle et al.*, 2014]:

$$\overline{u_j'\theta'} = \overbrace{-K_H \frac{\partial \overline{\theta}}{\partial x_j}}^{\text{local flux}} + \delta_{3j} W_{1D} \left[\overbrace{K_H \gamma}^{\text{nonlocal flux}} + \overbrace{\overline{w'\theta'}_{z_h} \left(\frac{z}{z_h} \right)^n}^{\text{explicit entrainment}} \right], \tag{20}$$

where $\overline{w'\theta'}_{z_h}$ is the heat flux at z_h [*Hong et al.*, 2006] and $n = 3$. Nonlocal terms (nonlocal heat flux + entrainment) are down weighted by W_{1D} as higher-resolution simulations better resolve turbulent heat flux and the large-eddies responsible for nonlocal heat transfer. The countergradient term follows [*Hong et al.*, 2006]

$$\gamma = b \frac{\overline{w'\theta'}_0}{w_{s0} z_h}, \tag{21}$$

where $b = 6.5$, $\overline{w'\theta'}_0$ the surface heat flux and w_{s0} is the mixed-layer velocity scale (w_s) at $z = 0.5 z_h$. Moreover, the simple explicit representation of entrainment, as presented in equation (20) based on *Noh et al.* [2003] and *Hong et al.* [2006] and implemented in the LEM following the methodology of *Boutle et al.* [2014], forms a simpler version of the blending scheme chosen for better comparison with the bounding approach.

3. Case Studies and Model Setup

Two case studies of a developing CBL were used to test the behavior of the subgrid schemes at grey zone resolutions. The Wangara experiment day 33 (16 August 1967) in Australia [*Clarke et al.*, 1971], a relatively deep BL development over dry land, is one of the most well-studied cases in BL meteorology [*Deardorff*, 1974; *Yamada and Mellor*, 1975; *André et al.*, 1978]. It has been also used recently for studying the nature of convective overturning at grey zone resolutions [*Zhou et al.*, 2014]. Here we follow the setup of the initial profiles and surface heat fluxes of *Yamada and Mellor* [1975] and *Zhou et al.* [2014]. Simulations start at 0900 local solar time (LST) and last for 9 h (1800 LST).

Another case adopted in this study is a measurement campaign that took place at the Met Office site on 16 April 2014. This case was a clear day (some thin cirrus clouds were present during early morning) with relatively light winds as the site was under the influence of a surface anticyclone stationed over central Europe. The observations consisted of a number of radiosondes from early morning to noon and a series of Doppler lidar scans to derive the flow field velocity variances over the site. Routine data of surface temperature and heat fluxes were also available during the measurement period. The initial temperature profile (at 0642 UTC) and the varying surface temperature boundary condition used in the Cardington simulations are presented in Figure 1. Further details of the Cardington surface site can be found in *Horlacher et al.* [2012] and *Osborne et al.* [2014].

A series of 3-D idealized runs were conducted using the LEM for the two case studies varying horizontal grid spacing from 50 to 3200 m using the Smagorinsky (SMAG), bounding (BOUND), and blending (BLEND) subgrid parametrizations. A periodic model domain of 9.6×9.6 km^2 with at least 24 horizontal grid points was used for both cases setting the model top at 2500 m for the Wangara and 2000 m for the Cardington case study. Horizontal resolutions in this study are chosen to adequately represent a range of grey zone resolutions based on the evolution of dominant length scales compared to the grid spacing. A damping layer was applied above 2000 m for the Wangara case. A vertical grid spacing (Δz) of 20 m was used for the $\Delta x = 50$ m runs and $\Delta z = 40$ m for all other simulations. The vertical resolution was chosen to be similar to the configuration of most regional models such as the MetUM UKV. LES converging runs [*Sullivan and Patton*, 2011] with $\Delta x = 25$ m ($\Delta z = 10$ m) showed that first-order quantities were identical to the 50 m simulations, while second-order quantities exhibited slight, nonsignificant differences in both cases.

Since the Wangara case has been extensively used for validation purposes over the past, no comparison will be made with available data in this study [see also *Zhou et al.*, 2014]. However, in order to configure the control 50 m run using SMAG (LES run hereafter) for the Cardington case, model results were compared with the available data set. Simulations started at 0645 UTC and lasted for 5.5 h with a slightly modified initial potential

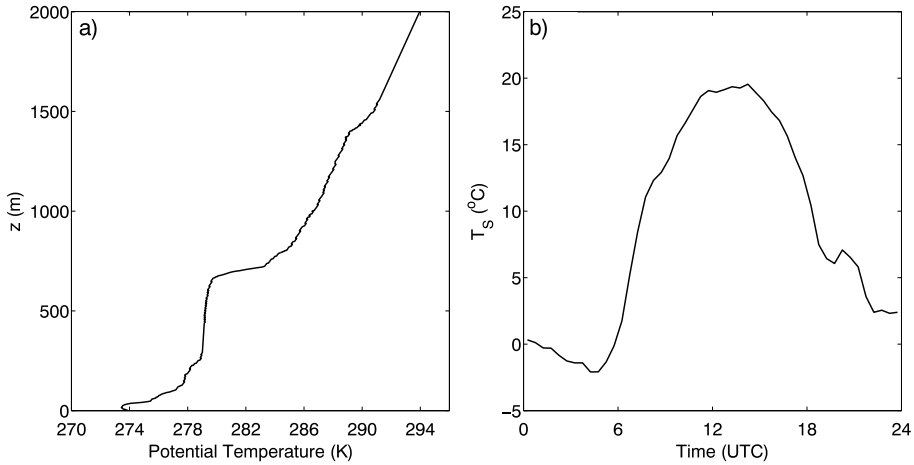

Figure 1. (a) Initialization sounding of potential temperature (16 April 2014 0642 UTC) for Cardington runs. (b) The 24 h evolution of surface temperature for the same day.

temperature profile compared to the 0642 UTC sounding (Figure 1) incorporating a 100 m deep mixed layer (ML) to allow for the fast model spin-up (see also *Kosović and Curry* [2000], for a stable BL case). Additionally, all simulations were forced by constant geostrophic winds ($U_g = -3\text{ms}^{-1}, V_g = 5\text{ms}^{-1}$) representative of the mean wind above the BL to avoid the development of some instabilities in the coarser runs that were noted due to the enhanced wind shear when the actual jet-shaped early morning wind profile was used.

Figure 2 shows the comparison of the domain-averaged simulated potential temperature profiles for the LES Cardington run with the actual radiosondes together with the estimated z_h from the soundings and model results (derived as the height where max[dθ/dz]). The LES run is able to reproduce the observed profiles and BL depth especially at 0921 and 1017 UTC. At earlier times (0738 and 0825 UTC) even though the profile shape and BL depth are well simulated, LES profiles exhibit a warm bias. This is due to the choice of the geostrophic vertical wind profile that produces stronger heat fluxes (not shown) in the early simulation hours. At the time of the last sounding (1114 UTC) observations show a pronounced heating of the lower troposphere probably due to warm advection that LES without the necessary large-scale forcing cannot reproduce remaining colder than the sounding. Moreover, z_h (see Figure 2b) is decreased denoting that the warm air advected over the site is suppressing turbulence and as a result BL development. Overall, the LES run is able to simulate the development of the shallow CBL over the Cardington site forced only by the local surface heat and momentum fluxes.

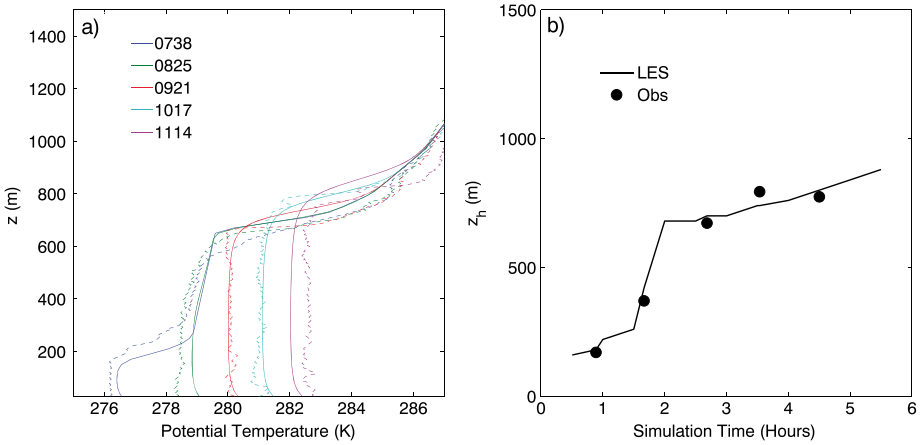

Figure 2. Comparison of (a) potential temperature soundings (dashed lines) and LES ($\Delta x = 50$ m) domain-averaged profiles (solid lines). (b) BL depth (z_h) derived from soundings (Obs) and LES run for the Cardington site simulations.

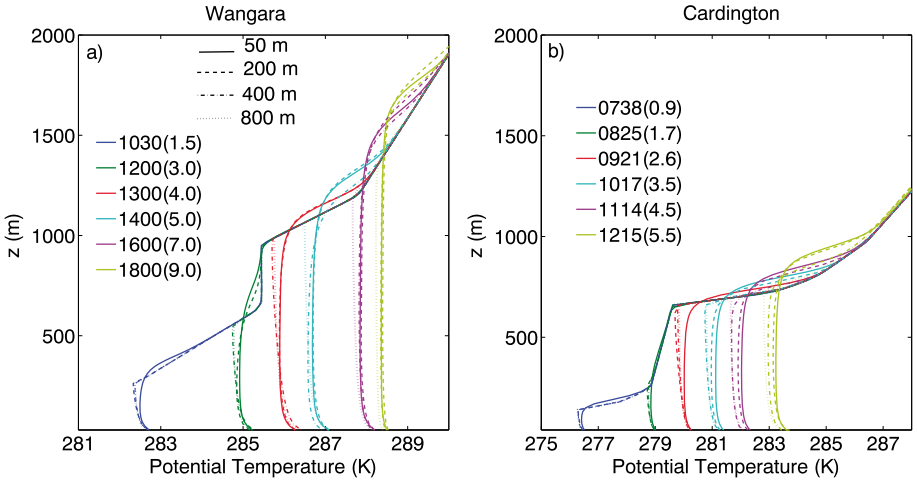

Figure 3. Evolution of domain-averaged potential temperature profiles from (a) Wangara (time in LST) and (b) Cardington (time in UTC) simulations for 50 m LES (solid lines), 200 m (dashed lines), 400 m (dashed-dotted lines), and 800 m (dotted lines) grid spacing. Simulation time is shown inside the parenthesis.

4. Model Results Across the Scales

4.1. Control SMAG Simulations

Figure 3 presents the domain-averaged potential temperature profiles from the SMAG simulations for the Wangara (Figure 3a) and Cardington (Figure 3b) case studies. In the early morning (1030 LST) none of the simulations can reproduce the LES (Δx = 50 m) temperature profile, exhibiting a slightly superadiabatic profile. During the course of the integration all simulations are gradually producing adiabatic profiles at different times with the coarser resolution runs delaying most. The simulations also start to resolve entrainment as the potential temperature profiles exhibit a distinctive cooling relative to the initial profile above the ML. The Δx = 800 m run is only producing a well-mixed profile at the end of the simulation (1800 LST) while remaining slightly colder than the other runs. For the shallower Cardington BL case (Figure 3b), adiabatic profiles take longer to develop and by 1215 UTC the 800 m run is still not able to reproduce the LES profile. As a result of the delay, the Δx = 400 m and 800 m simulations are not able to match LES results, exhibiting colder potential temperatures through the whole depth of the CBL. The Smagorinsky scheme behaves similar to a local BL scheme at these grid spacings unable to provide any countergradient fluxes resulting in superadiabatic profiles due to poor mixing. It should be noted that according to the lidar data, the BL over Cardington did not develop much after 1215 UTC and collapsed after 1600 UTC due to the negative surface heat fluxes (not shown).

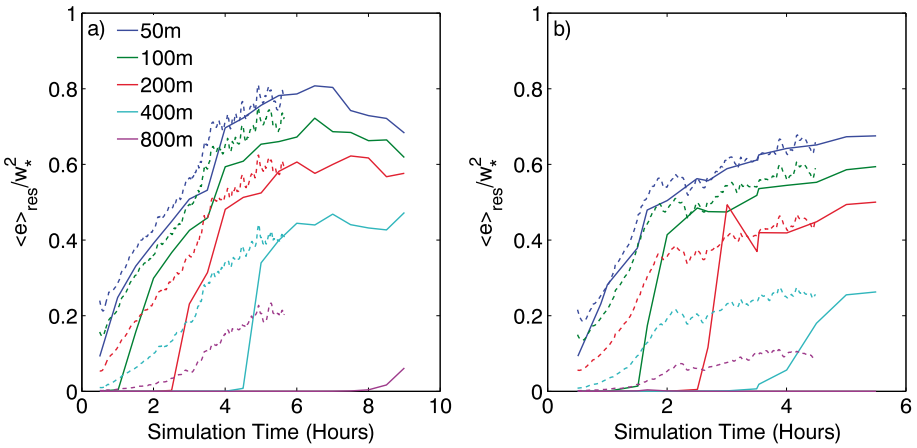

Figure 4. Resolved domain-averaged TKE ($< e_{res} >$) normalized by w_*^2 in the middle of the BL from coarse-grained LES (50 m) fields (dashed lines) and SMAG simulations (solid lines) from (a) Wangara and (b) Cardington runs for different horizontal resolutions.

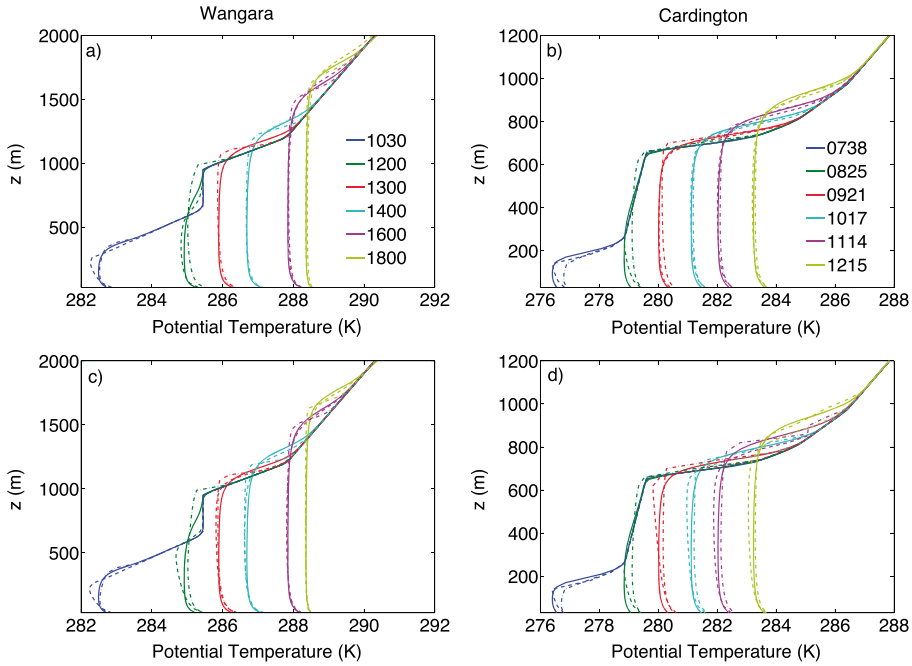

Figure 5. Evolution of domain-averaged potential temperature profiles from LES 50 m run (solid lines) compared to BOUND (dashed lines) and BLEND (dashed-dotted lines) runs for (a) Wangara $\Delta x = 400$ m, (b) Cardington $\Delta x = 400$ m, (c) Wangara $\Delta x = 800$ m, and (d) Cardington $\Delta x = 800$ m case studies.

The behavior of the domain-averaged temperature profiles can be explained by examining the time-dependent TKE in the middle of the BL ($z/z_h = 0.5$) and comparing with the TKE from the coarse-grained LES fields at the corresponding resolutions [see *Efstathiou and Beare*, 2015] as shown in Figure 4. Turbulence initiation is significantly delayed in both cases for simulations with $\Delta x > 100$ m (reaching up to 4 and 8 h for the 400 and 800 m Wangara runs, respectively), while exhibiting an abrupt onset at intermediate resolutions compared to the coarse-grained derived TKE. For the Cardington 800 m run, no TKE is resolved at least until the end of simulation time. However, at the onset of resolved TKE, simulations start to resolve some convective overturning that acts as the nonlocal component of the sensible heat flux, gradually neutralizing potential temperature profiles. This can be clearly seen in Figure 3a for the Wangara case, where after 1400 LST profiles from the 400 m run become well mixed, explicitly resolving entrainment processes which coincide with the onset of resolved TKE after about 4 h of simulation time (see Figure 4a). The Cardington simulations also exhibit the same characteristics especially the 200 and 400 m runs after 1017 and 1114 UTC, respectively (see Figures 3b and 4b). The above findings are in accordance with *Zhou et al.* [2014] and *Ching et al.* [2014] that demonstrated the delay in the initiation of convection at grey zone resolutions as a function of the grid-dependent Rayleigh number.

4.2. The BOUND and BLEND Approaches at Grey Zone Resolutions

The domain-averaged potential temperature profiles from the BLEND and BOUND $\Delta x = 400$ and 800 m runs for the two morning CBL development cases are presented in Figure 5. The BOUND approach produces similar temperature profiles to the SMAG runs when the BL is shallow and cannot reproduce the LES profiles for either case. As the CBL deepens, the 400 m simulations using BOUND match the LES profiles early in the simulations for both cases (Figures 5a and 5b). The BOUND approach is able to reproduce the whole vertical distribution of potential temperature: in the surface, mixed layer, and entrainment zone. The Wangara 800 m simulation takes longer to develop the well-mixed profiles (Figure 5c), while the corresponding Cardington run (see Figure 5d) delays even more, not being able to fully reproduce the LES.

The BLEND scheme is able to match LES temperature profiles during the shallow stage of the CBL evolution in both cases as the blending function (equation (15)) is close to 1 as seen in Figure 6 and the scheme behaves similar to a 1D nonlocal BL parametrization. However, after the rapid mixed-layer development (3–4 h of simulation time), the blending function for the 400 m runs drops to values of 0.6 for the Wangara and 0.7 for the Cardington case. This seems to have a profound impact on potential temperature that exhibits a slightly

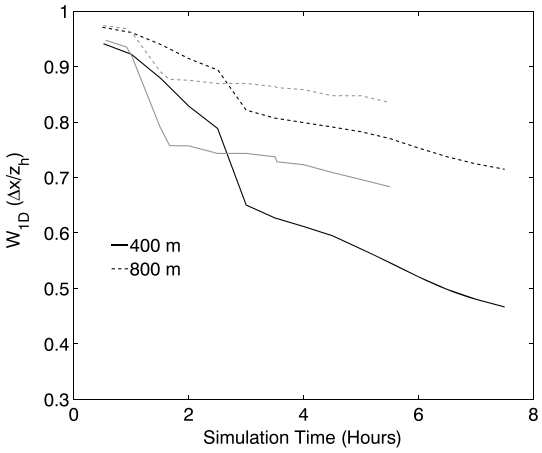

Figure 6. Evolution of the blending function (W_{1D}) used in the BLEND 400 m and 800 m runs for the Wangara (black line) and Cardington (grey line) cases.

superadiabatic profile (1300 LST for the Wangara and 0921 UTC for the Cardington case, Figures 5a and 5b) as the subgrid nonlocal contribution is reduced to 60–70% of the total heat flux. In the 800 m runs (Figures 5c and 5d) this effect is not so pronounced as the values of the blending function do not fall below 0.8 after 4 h of simulation time in both cases (see Figure 6).

Figure 7 is showing the time-dependent resolved TKE from the BOUND and BLEND simulations in the middle of the BL, together with the control SMAG 400 and 800 m simulations and the corresponding resolved TKE from the coarse-grained fields. The BOUND simulations are able to follow the TKE evolution from the coarse-grained fields, spinning up significantly faster than BLEND and SMAG especially in the deep Wangara CBL. The BLEND runs do not improve spin-up substantially compared to the control SMAG simulations (except in the 800 m Wangara run), in accordance with the findings of *Shin and Hong* [2015]. It is also obvious from Figure 7 that the BLEND scheme is underestimating the resolved TKE [*Honnert et al.*, 2011; *Shin and Hong*, 2013] compared to the coarse-grained fields although during the late stages of the CBL development TKE is increasing in the Wangara case. During the late CBL development, the nonlocal heat flux contribution (countergradient and explicit entrainment terms) has been almost reduced by 50% (see blending function, Figure 6). This can be seen also in the partitioning of the vertical heat flux for the Wangara case study ($\Delta x = 400$ m) as shown in Figure 8. At 1030 LST (1.5 h of simulation time) the SMAG run produces only subgrid local heat flux without any nonlocal contribution (Figure 8a), while the BLEND scheme parametrizes the nonlocal fluxes and explicitly represents entrainment as a conventional 1D nonlocal scheme (Figure 8b). The BOUND approach is similar to SMAG with some resolved heat flux starting to emerge in the simulation (Figure 8c). As the CBL deepens (1300 LST), the BOUND run resolves some of the convective overturning that acts as the nonlocal transport (Figure 8f). In the BLEND simulation (Figure 8e) the countergradient flux and especially parametrized entrainment are reduced due to the decreasing values of the blending function. As there is very little resolved turbulence, the total nonlocal transport is also reduced compared to the BOUND run. It should be noted that the potential temperature profile at 1300 LST is slightly superadiabatic (see Figure 5a) indicating the lack of nonlocal mixing. Heat flux is still unresolved after 4 h in the SMAG run (Figure 8d), while after 7 h of simulation time (Figure 8g) the vertical heat flux becomes similar to BOUND (Figure 8i). At the same time BLEND simulation is resolving convection (Figure 8h), less intense compared to BOUND (Figure 8i); however, the sum of the subgrid and resolved flux matches the BOUND run.

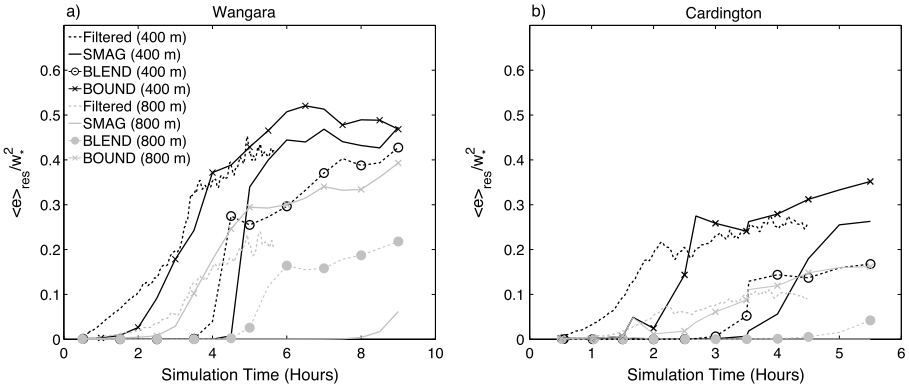

Figure 7. Domain-averaged resolved TKE ($< e >_{res}$) normalized by w_*^2 in the middle of the BL from coarse-grained (filtered) LES, SMAG, BOUND, and BLEND simulations from (a) Wangara and (b) Cardington runs for the 400 m and 800 m grid spacing.

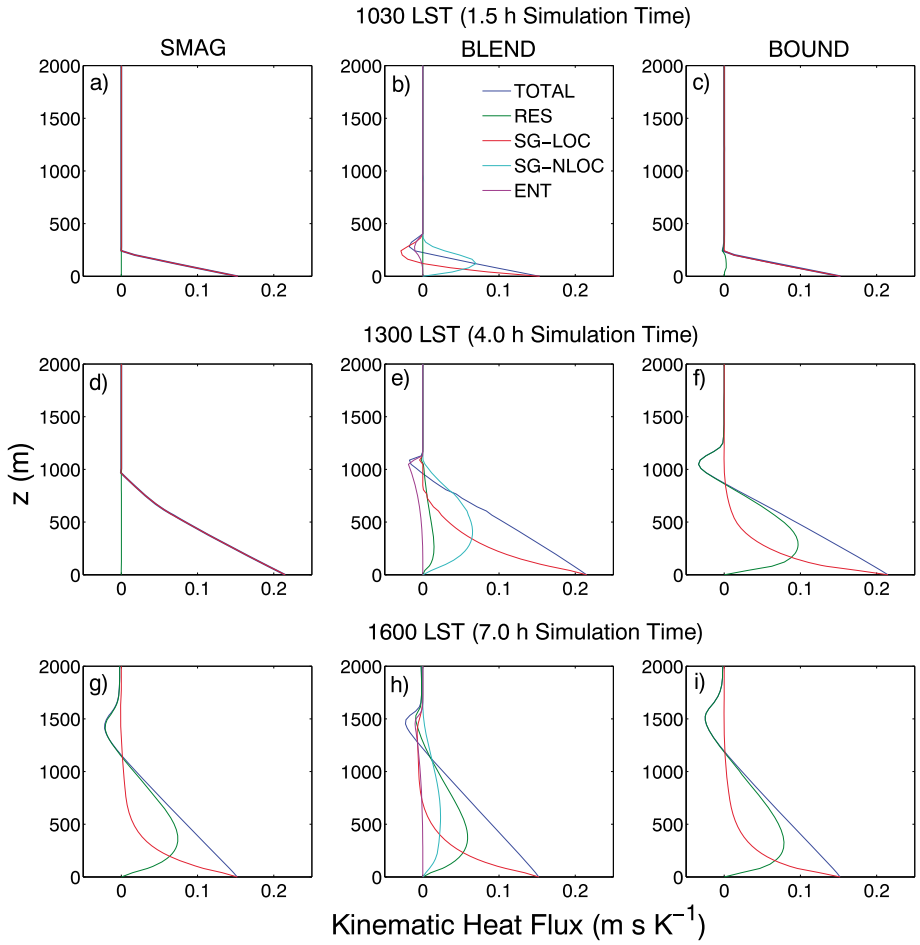

Figure 8. Partitioning of the domain-averaged sensible heat flux to total (TOTAL), resolved (RES), local subgrid (SG-LOC), nonlocal subgrid (SG-NLOC), and entrainment (ENT) heat fluxes for the 400 m Wangara (a) 1030 LST SMAG, (b) 1030 LST BLEND, (c) 1030 LST BOUND, (d) 1300 LST SMAG, (e) 1300 LST BLEND, (f) 1300 LST BOUND, (g) 1600 LST SMAG, (h) 1600 LST BLEND, and (i) 1600 LST BOUND simulations.

In Figure 9, the domain-averaged profile of the vertical velocity variance ($\overline{w}'^2$) from BOUND and BLEND simulations is compared with the reference (coarse-grained) velocity variance profiles at $\Delta x = 400$ m and 800 m resolutions for the Cardington case. At first, as shown in Figure 9a, the LES variance profiles are validated against lidar measurements for different times over Cardington site. LES can successfully reproduce vertical velocity variance and the subsequent increase in the turbulent intensity during the morning CBL development; however, lidar data show that turbulence is suppressed near noon (1145 UTC). LES cannot reproduce this feature that is probably due to the warm air advection over the site at that time as mentioned in section 2 (see Figure 2). The vertical profile of vertical velocity variance from the BOUND and BLEND 400 m and 800 m simulations is compared with the coarse-grained LES variance at 0925 UTC in Figures 9b and 9c. BOUND is able to follow the shape and magnitude of the reference profiles, while BLEND run is still not resolving any vertical velocity fluctuations providing another illustration of the delayed spin-up problem (see also Figure 7b).

Finally, Figure 10 shows the CBL depth output from the BLEND and BOUND schemes together with the diagnosed z_h from the LES run (height of minimum vertical heat flux). Both approaches are in overall agreement with the LES, although the current implementation of the BLEND scheme exhibits a slight overestimation of z_h especially in the Wangara case.

5. Discussion on Turbulence Onset at Grey Zone Resolutions

The control SMAG simulations at grey zone resolutions resolve convective motions whose onset and intensity depend on grid spacing. Similar to the findings of *Zhou et al.* [2014] and *Ching et al.* [2014], there is a

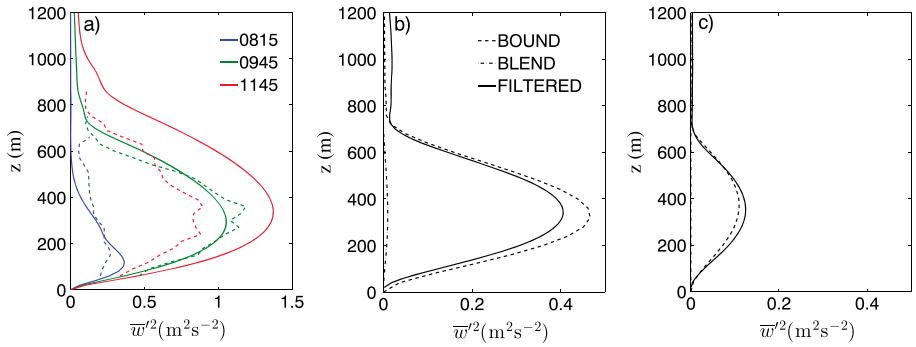

Figure 9. (a) Comparison of measured vertical velocity variance ($\overline{w}'^2$) from lidar data (dashed lines, averaged every 15 min) with the LES run (solid lines) for the Cardington case for different times (UTC). (b) Comparison of $\overline{w}'^2$ from the BOUND and BLEND 400 m runs with the corresponding filtered (coarse-grained) $\overline{w}'^2$ from the LES fields. (c) Same as Figure 9b but for the 800 m runs.

significant delay in the development of convective overturning in the control SMAG simulations until temperature gradients become steep enough to trigger convection. In the context of the evolving CBL, dominant length scales are constantly changing compared to the quasi-steady BL simulations where the objective is to allow necessary spin-up to reach equilibrium and maintain an almost constant TKE. To illustrate the importance of turbulence onset in the developing CBL, Figure 11 presents a log-log plot of the resolved TKE at $z/z_h = 0.5$ from the Wangara case as derived from the coarse-grained fields, as a function of the similarity variable $\Delta x/z_h$ [*Honnert et al.*, 2011]. The resolved TKE from the BOUND and BLEND, 400 m and 800 m runs, is also shown in Figure 11. The plot is divided into three different regimes according to the value of $\Delta x/z_h$: the LES, grey zone, and mesoscale region. The onset of the grey zone is defined according to *Beare* [2014] using a dissipation length scale (l_d) to diagnose the resolutions at which dissipation controls TKE production. *Beare* [2014] defined the grey zone at $z_h/l_d < 0.7$, obtained by running the LEM with different resolutions and using the standard 3-D Smagorinsky scheme. Similarly, Wangara CBL SMAG simulations converge to this value (not shown) at $\Delta x/z_h \approx 0.3$ which is considered the grey zone onset for this case. The mesoscale limit is set rather arbitrarily at $\Delta x/z_h = 4$, while a threshold value for resolved TKE is set at 0.01 $\mathrm{m^2s^{-2}}$.

Figure 11 shows that even the 50 m run starts from the grey zone limit when BL is really shallow, and as z_h increases, the simulation lies entirely in the LES regime. The coarse-grained fields at $\Delta x = 100$ m and 200 m

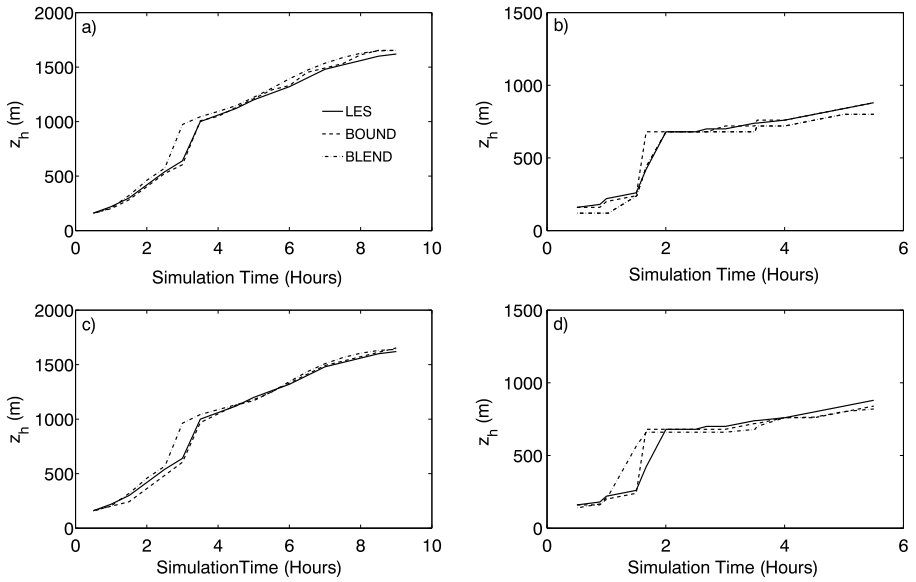

Figure 10. (a) CBL depth diagnosed from the LES runs as a function of simulation time compared to BOUND and BLEND schemes for the (a) Wangara 400 m simulations, (b) Cardington 400 m, (c) Wangara 800 m, and (d) Cardington 800 m.

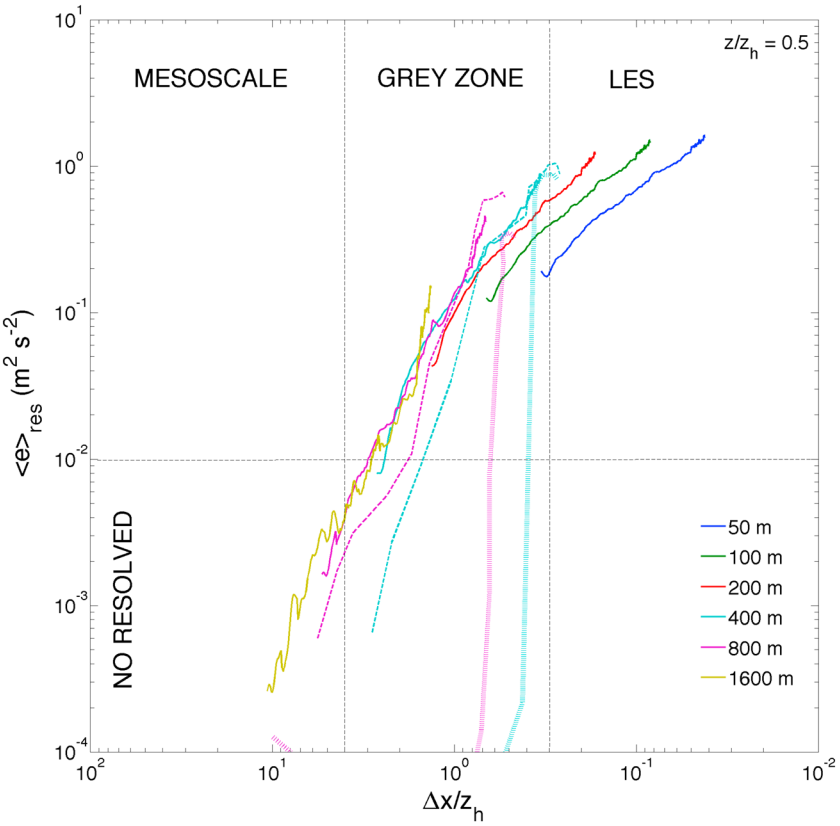

Figure 11. Domain-averaged resolved TKE ($< e >_{res}$) in the middle of the BL from coarse-grained LES (50 m) fields (solid lines), BOUND (dashed lines), and BLEND (dotted lines) simulations from the Wangara case as a function of $\Delta x/z_h$ for different horizontal resolutions.

resolve TKE initially in the grey zone region, while during the rapid CBL development is found to lie in the LES regime. In contrast, TKE from the 400 m and 800 m filtered fields lies in the grey zone starting from almost an unresolved state (especially the 800 m case which initiates from the mesoscale limit). At 1600 m very little resolved TKE is observed in the coarse-grained fields only when the simulation enters the grey zone regime. It becomes obvious from Figure 11 that even though simulations have a specified grid spacing, the evolving turbulence scales expressed by z_h during the CBL development control the ability of the grid to resolve convection. Moreover, any misrepresentation of the flow field in the early stages of the simulation will be carried along during the course of integration, as illustrated by the spin-up problems or unrealistic structures found in the deep mixing layer [*Zhou et al.*, 2014; *Ching et al.*, 2014].

Furthermore, comparing resolved TKE from the coarse-grained fields with the simulations shows that BOUND runs are only able to resolve turbulent fluctuations when $\Delta x/z_h < 2$. The BOUND approach is based on leading model dynamics to resolve convection in a way that imitates the filtered fields [see *Efstathiou and Beare*, 2015]. However, for $\Delta x/z_h > 2$ coarse-grained fields exhibit almost no convective overturning [*Honnert et al.*, 2011; *Shin and Hong*, 2013; *Efstathiou and Beare*, 2015], and BOUND is unable to account for nonlocal heat transfer when the BL is shallow. As a result, temperature profiles are not well represented during early morning in the Wangara and Cardington case, while the same is apparent for the whole 800 m Cardington run using BOUND. The BLEND runs start to resolve TKE near the LES limit without significantly improving the spin-up compared to the SMAG runs. In fact, all SMAG runs with $\Delta x > 100$ m, as well as the BLEND runs performed here, resolve TKE only when $\Delta x/z_h < 0.4$ (not shown).

6. Concluding Remarks

In this study, two approaches in parametrizing turbulence at grey zone resolutions are implemented in the LEM and compared with the standard 3-D Smagorinsky scheme in simulating the CBL morning development. The Wangara experiment day 33 and a case study from the Met Office Cardington measurement site serve

as a test bed to perform the simulations. The LEM is able to reproduce first- and second-order quantities at LES resolutions compared to radiosonde and lidar measurements from the Cardington site. Coarsening grid resolution results in gradually increasing spin-up time followed by the abrupt onset of resolved TKE for both cases. In the absence of resolved fluctuations potential temperature profiles become superadiabatic due to the lack of nonlocal heat transfer.

The simpler implementation of the blending scheme is able to follow LES results especially when the BL is shallow and the scheme behaves as a nonlocal 1D parametrization. However, simulation spin-up is not substantially improved compared to the Smagorinsky scheme. The spin-up issue is manifested during the rapid ML growth (especially for simulations with $\Delta x = 400$ m) when the blending function reduces the contribution of the parametrized nonlocal flux and entrainment, producing slightly superadiabatic profiles. The magnitude and timing of resolved TKE do not match the coarse-grained fields, although resolved TKE increases with the reduced contribution of parametrized fluxes. Overall, the blending scheme sufficiently matches the potential temperature profiles, particularly in the shallow Cardington case BL.

The bounding approach is able to reproduce the time evolution of the reference TKE from the coarse-grained fields, especially the onset of resolved TKE compared to SMAG and BLEND runs. Additionally, vertical velocity variance derived from the coarse-grained fields is well captured by the BOUND simulations. Potential temperature profiles match LES through the whole depth of the BL mainly during and after the rapid ML development. This is in accordance with the findings of *Efstathiou and Beare* [2015] which showed the ability of the bounding scheme in maintaining the resolved TKE and the characteristics of the coherent turbulence structures in agreement with the reference fields at grey zone resolutions. However, as the BOUND runs are unable to resolve TKE for $\Delta x/z_h > 2$, the bounding scheme does not provide any significant improvement compared to the standard Smagorinsky scheme when the BL is shallow.

The evolving scales in the developing CBL show that, regardless of grid resolution, the simulations go through different regimes exhibiting the challenges of modeling the diurnal cycle of convection realistically at grey zone resolutions. Only convergent LES lies entirely in the LES region [*Sullivan and Patton*, 2011]. All simulations except BOUND start to resolve TKE only as they approach the LES limit ($\Delta x/z_h < 0.4$). The implications of grid-scale convection are shown in the delaying turbulence onset that affects the shape and evolution of the potential temperature profiles during the morning CBL development. This inaccurate representation of first- and second-order quantities in the BL would be expected to affect the development of shallow convective clouds and the transition to deep convection in realistic NWP applications.

The two approaches implemented in the LEM and presented here are able to improve the simulation of the evolving CBL. From a practical standpoint, both methods exhibit particular strengths and weaknesses, indicating the level of compromise that needs to be made currently in high-resolution NWP: BLEND reproduces the LES vertical profiles through the BL development but seriously delays the spin-up of turbulence, failing to produce the level of resolved turbulence compared to the coarse-grained fields, which affects the vertical profiles later on. Alternatively, BOUND follows the reference resolved TKE as the BL evolves, matching the vertical LES profiles after the onset of resolved TKE, but this is excited by generating unrealistic superadiabatic profiles early on. Therefore, developing a method to inject and maintain a realistic amount of resolved turbulence at the very early stages of the simulations [e.g., *Muñoz-Esparza et al.*, 2014; K. Kober and G. C. Craig, Stochastic boundary layer perturbations to represent uncertainty in convective initiation, in review to *Journal of the Atmospheric Sciences*, 2015] would potentially improve the behavior of both parametrizations at grey zone resolutions.

Acknowledgments
This work has been funded by the Natural Environment Research Council (NERC) GREYBLS (Modelling Grey Zone Boundary Layers) project (grant NE/K011456/1). We acknowledge the use of the MONSooN system, a collaborative facility supplied under the Joint Weather and Climate Research Programme, which is a strategic partnership between the Met Office and the Natural Environment Research Council. We would like to thank the anonymous reviewers for their constructive comments that improved this paper. The data used are listed in the references and included in the figures of this paper.

References

André, J. C., G. De Moor, P. Lacarrère, and R. du Vachat (1978), Modeling the 24-hour evolution of the mean and turbulent structures of the planetary boundary layer, *J. Atmos. Sci.*, *35*(10), 1861–1883, doi:10.1175/1520-0469(1978)035<1861:MTHEOT>2.0.CO;2.

Arakawa, A., and C.-M. Wu (2013), A unified representation of deep moist convection in numerical modeling of the atmosphere. Part I, *J. Atmos. Sci.*, *70*(7), 1977–1992, doi:10.1175/JAS-D-12-0330.1.

Beare, R. (2014), A length scale defining partially-resolved boundary-layer turbulence simulations, *Boundary Layer Meteorol.*, *151*(1), 39–55, doi:10.1007/s10546-013-9881-3.

Boutle, I. A., J. E. J. Eyre, and A. P. Lock (2014), Seamless stratocumulus simulation across the turbulent gray zone, *Mon. Weather Rev.*, *142*(4), 1655–1668, doi:10.1175/MWR-D-13-00229.1.

Brown, A. R. (1999), The sensitivity of large-eddy simulations of shallow cumulus convection to resolution and subgrid model, *Q. J. R. Meteorol. Soc.*, *125*(554), 469–482, doi:10.1002/qj.49712555405.

Brown, A. R., S. H. Derbyshire, and P. J. Mason (1994), Large-eddy simulation of stable atmospheric boundary layers with a revised stochastic subgrid model, *Q. J. R. Meteorol. Soc.*, *120*(520), 1485–1512, doi:10.1002/qj.49712052004.
Charney, J., R. Fjörtoft, and J. Neumann (1950), Numerical integration of the barotropic vorticity equation, *Tellus A*, *2*(4), 237–254.
Ching, J., R. Rotunno, M. LeMone, A. Martilli, B. Kosovic, P. A. Jimenez, and J. Dudhia (2014), Convectively induced secondary circulations in fine-grid mesoscale numerical weather prediction models, *Mon. Weather Rev.*, *142*(9), 3284–3302, doi:10.1175/MWR-D-13-00318.1.
Clarke, R. H., A. J. Dyer, R. R. Brook, D. G. Reid, and A. J. Troup (1971), The Wangara experiment: Boundary layer data, *Tech. Rep. 340*, CSIRO Div. of Meteorol. Phys. Tech., Australia.
Deardorff, J. (1974), Three-dimensional numerical study of turbulence in an entraining mixed layer, *Boundary Layer Meteorol.*, *7*(2), 199–226, doi:10.1007/BF00227913.
Efstathiou, G. A., and R. J. Beare (2015), Quantifying and improving sub-grid diffusion in the boundary-layer grey zone, *Q. J. R. Meteorol. Soc.*, *141*(693), 3006–3017, doi:10.1002/qj.2585.
Holtslag, A. A. M., and B. A. Boville (1993), Local versus nonlocal boundary-layer diffusion in a global climate model, *J. Clim.*, *6*(10), 1825–1842, doi:10.1175/1520-0442(1993)006<1825:LVNBLD>2.0.CO;2.
Hong, S.-Y., and H.-L. Pan (1996), Nonlocal boundary layer vertical diffusion in a medium-range forecast model, *Mon. Weather Rev.*, *124*(10), 2322–2339, doi:10.1175/1520-0493(1996)124<2322:NBLVDI>2.0.CO;2.
Hong, S.-Y., Y. Noh, and J. Dudhia (2006), A new vertical diffusion package with an explicit treatment of entrainment processes, *Mon. Weather Rev.*, *134*(9), 2318–2341, doi:10.1175/MWR3199.1.
Honnert, R., V. Masson, and F. Couvreux (2011), A diagnostic for evaluating the representation of turbulence in atmospheric models at the kilometric scale, *J. Atmos. Sci.*, *68*(12), 3112–3131, doi:10.1175/JAS-D-11-061.1.
Horlacher, V., S. Osborne, and J. Price (2012), Comparison of two closely located meteorological measurement sites and consequences for their areal representativity, *Boundary Layer Meteorol.*, *142*(3), 469–493, doi:10.1007/s10546-011-9684-3.
Ito, J., H. Niino, M. Nakanishi, and C.-H. Moeng (2015), An extension of the Mellor-Yamada model to the terra incognita zone for dry convective mixed layers in the free convection regime, *Boundary Layer Meteorol.*, *157*(1), 23–43, doi:10.1007/s10546-015-0045-5.
Kosović, B., and J. A. Curry (2000), A large eddy simulation study of a quasi-steady, stably stratified atmospheric boundary layer, *J. Atmos. Sci.*, *57*(8), 1052–1068, doi:10.1175/1520-0469(2000)057<1052:ALESSO>2.0.CO;2.
Leonard, B. P., M. K. Macvean, and A. P. Lock (1993), Positivity-preserving numerical schemes for multidimensional advection, *Tech. Rep. 62*, NASA, Cleveland, Ohio.
Lock, A. P., A. R. Brown, M. R. Bush, G. M. Martin, and R. N. B. Smith (2000), A new boundary layer mixing scheme. Part I: Scheme description and single-column model tests, *Mon. Weather Rev.*, *128*(9), 3187–3199, doi:10.1175/1520-0493(2000)128<3187:ANBLMS>2.0.CO;2.
Muñoz-Esparza, D., B. Kosović, J. Mirocha, and J. van Beeck (2014), Bridging the transition from mesoscale to microscale turbulence in numerical weather prediction models, *Boundary Layer Meteorol.*, *153*(3), 409–440, doi:10.1007/s10546-014-9956-9.
Noh, Y., W. Cheon, S. Hong, and S. Raasch (2003), Improvement of the k-profile model for the planetary boundary layer based on large eddy simulation data, *Boundary Layer Meteorol.*, *107*(2), 401–427, doi:10.1023/A:1022146015946.
Osborne, S., S. Abel, I. Boutle, and F. Marenco (2014), Evolution of stratocumulus over land: Comparison of ground and aircraft observations with numerical weather prediction simulations, *Boundary Layer Meteorol.*, *153*(2), 165–193, doi:10.1007/s10546-014-9944-0.
Pearson, K. J., G. M. S. Lister, C. E. Birch, R. P. Allan, R. J. Hogan, and S. J. Woolnough (2014), Modelling the diurnal cycle of tropical convection across the 'grey zone', *Q. J. R. Meteorol. Soc.*, *140*(679), 491–499, doi:10.1002/qj.2145.
Piacsek, S. A., and G. P. Williams (1970), Conservation properties of convection difference schemes, *J. Comput. Phys.*, *6*(3), 392–405, doi:10.1016/0021-9991(70)90038-0.
Shin, H. H., and S.-Y. Hong (2013), Analysis of resolved and parameterized vertical transports in convective boundary layers at gray-zone resolutions, *J. Atmos. Sci.*, *70*(10), 3248–3261, doi:10.1175/JAS-D-12-0290.1.
Shin, H. H., and S.-Y. Hong (2015), Representation of the subgrid-scale turbulent transport in convective boundary layers at gray-zone resolutions, *Mon. Weather Rev.*, *143*(1), 250–271, doi:10.1175/MWR-D-14-00116.1.
Sullivan, P. P., and E. G. Patton (2011), The effect of mesh resolution on convective boundary layer statistics and structures generated by large-eddy simulation, *J. Atmos. Sci.*, *68*(10), 2395–2415, doi:10.1175/JAS-D-10-05010.1.
Troen, I., and L. Mahrt (1986), A simple model of the atmospheric boundary layer; sensitivity to surface evaporation, *Boundary Layer Meteorol.*, *37*(1–2), 129–148, doi:10.1007/BF00122760.
Wyngaard, J. C. (2004), Toward numerical modeling in the "terra incognita", *J. Atmos. Sci.*, *61*(14), 1816–1826, doi:10.1175/1520-0469(2004)061<1816:TNMITT>2.0.CO;2.
Yamada, T., and G. Mellor (1975), A simulation of the Wangara atmospheric boundary layer data, *J. Atmos. Sci.*, *32*(12), 2309–2329, doi:10.1175/1520-0469(1975)032<2309:ASOTWA>2.0.CO;2.
Zhou, B., J. S. Simon, and F. K. Chow (2014), The convective boundary layer in the terra incognita, *J. Atmos. Sci.*, *71*(7), 2545–2563, doi:10.1175/JAS-D-13-0356.1.